Surrogate-based aerodynamics for composite wing box sizing

Bordogna, Marco Tito; Bettebghor, Dimitri; Blondeau, Christophe; De Breuker, Roeland

Surrogate-based Aerodynamics for Composite Wing Box Sizing

Marco Tito Bordogna[1,2], Dimitri Bettebghor[1], Christophe Blondeau[1] and Roeland De Breuker[2]

[1] *ONERA, The French Aerospace Lab, F-92322 Châtillon, France*
[2] *Faculty of Aerospace Engineering, Delft University of Technology, 2629 HS Delft, The Netherlands*

Abstract

The main objective of this paper is to propose an aeroelastic optimization approach capable of performing structural sizing optimization considering structural and aerodynamic constraints. The proposed approach uses a detailed FE model of a composite wing with shell elements in order to obtain realistic weight estimation and structural responses. Moreover, a surrogate model based on rigid RANS computations provides a high-fidelity lift and drag coefficient estimation during the optimization as constraints. The use of RANS computations allows the surrogate model to consider all drag components and not the induced drag only. An approximation of the structural displacement is proposed based on modal projection and principle component analysis. Results shows that a polynomial regression of order four is accurate enough to be used as surrogate model of the drag coefficient and of the lift-to-drag ratio. Moreover, it is possible to conclude that improvements in aerodynamic performance, with fixed aerodynamic shape, comes at the price of a heavier and stiffer structure.

Keywords: Aeroelasticity, Optimization, Surrogate, Aerodynamics, Composite

1 Introduction

Composite materials, thanks to their anisotropy and their high stiffness-to-weight and strength-to-weight ratios, are being used increasingly in many industries and especially in the aerospace sector. Composite superior characteristics allow design engineers to explore novel configurations [1] and to redesign conventional structure to further improve performance by tailoring the material anisotropy [16, 5]. As seen in recent wing development (i.e. 777-X), there is a tendency in designing lighter, longer and more flexible wings. One of the reason behind this is to reduce the span loading that is linked to induced drag. Moreover, thanks to composite anisotropy, the span-wise lift distribution can be improved by proper optimizing the material anisotropy. For these reasons, but also to account for potential aeroelastic instabilities (e.g. flutter), fluid-structure interaction need to be taken into account even during early design phase together with composite optimization.

Different fidelity levels could be used to perform aeroelastic computations depending on the design phase and the requested responses: from Euler-Bernoulli beam structures with panel methods for unsteady aerodynamics [11], to complex FEM shell geometry fully coupled with high-fidelity RANS computations [10]. Panel methods, like vortex lattice method (VLM) or doublet lattice method (DLM), are very common during early design phase due to their fast computation time and easy modeling that make them ideal for early optimizations. However, panel methods are irrotational and inviscid thus unsuitable to estimate aircraft performance (i.e lift-to-drag ratio or drag coefficient). On the other hand, RANS model can be used to calculate aircraft performance but at the price of very computational expensive calculations, limiting their use in optimization even with current supercomputer. A very popular alternative to the direct use of CFD in optimization processes, is to construct a cheap to compute approximation model of the expensive CFD analysis solver. These approximation models are usually referred to as surrogate models or metamodels. The surrogate model expresses complicated relationships between the response (output) and the design variables (input) with a relatively simple equation. Once computed, this model requires very little computational effort to run making them ideal for optimization purposes.

Several authors used surrogate models to perform static aero-structural optimization. Zhang et al. [20] compared different surrogate models (quadratic polynomial regression, Kriging and neural network) with the objective of maximizing the aircraft lift-to-drag ratio and minimizing the weight as function of wing planform parameters and structural thicknesses and concluded that not considering the aeroelastic effect will result in large errors. Rasmussen et al. [15] outlines a methodology to optimize the weight and perform design exploration for a joined-wing aircraft. The optimization has been divided in two steps, where the first step consists of performing aerostructural optimization (no drag involved in the objective function) for weight minimization for different geometric aircraft configuration. A weight-optimized solution was found by varying spar, rib, and skin thicknesses of the wing structure. The second step consisted of creating an approximation, via polynomial regression, of the entire design space using the optimized structures as sample points. The surrogate moderate fit is then used to define optimal regions and design trends and not use to determine precise optimal configuration. Paiva et al. [13] also compares different surrogate models (quadratic polynomial regression, Kriging and neural network) of the aerodynamic coefficients (C_L, C_D and C_M) as function of several geometrical, structural (thicknesses) and aerodynamic (NACA) parameters concluding that polynomial regression prove to be adequate only for low dimensionality problems. Lebofsky et al. [11] utilizes surrogate model to optimize the drag coefficient of an aircraft wing as function of the jig twist-law and deflection parameters of trailing edge flaps.

In all above mentioned works surrogate models have been used to approximate aerodynamic quantities (C_L, C_D, C_M or C_L/C_D) as function of wing planform geometrical parameters, aerodynamic parameter (NACA profile variables) and structural thicknesses. In the present work, a composite wing box is optimized with respect to thickness and parameters modeling the composite anisotropy (i.e. lamination parameters) of its different panels and therefore considering the effect of the composite anisotropy in the optimization with the intent of tailoring it. A surrogate model based on rigid CFD simulations, as function of wing displacement during maneuvers or cruise conditions, is introduced to take aerodynamic performance into account. The ONERA CFD solver *elsA* [4] is used to perform all aerodynamic computations. However, using directly the wing displacement (u) as surrogate-model input would results in to many variables, therefore an approach to approximate the structural displacement and to reduce the number of variables is proposed.

The framework is presented in section 2 together with the displacement approximation, used to reduce the dimensions of the surrogate model input, and the surrogate models. Sections. 3 and 4 present respectively the test case and the optimization problems. Finally in section 5 the results are presented and commented.

2   Proposed Framework

The approach presented in this paper is built around the commercial FE tool MSC.Nastran. Its solution 144 is capable of computing static aeroelastic loads and sensitivities using the doublet lattice method (DLM) [7] and it is commonly used in the industry to perform aeroelastic optimization with structural constraints. However, aerodynamic performance cannot be properly captured due to the limitations of panel methods. The surrogate model is built from rigid RANS computations and provides the total wing drag coefficient and lift-to-drag ratio as a function of the wing displacement (u), that depends directly on the structural parameters (X). For example, if we consider a surrogate model of the drag coefficient C_D, it is possible to write it as:

$$\widehat{C}_D \approx f(u(X)) \tag{1}$$

2.1   Displacement approximation

Lets consider free-free structure subjected to a static load (F). In order to calculate the displacement at which the structure is subjected the system (Eq.2) have to be solved.

$$\mathbf{K}u = F \tag{2}$$

However, in the case of a free-free structure $\mathbf{K}$ is singular and the system cannot be solved as it is [6]. From a mechanical prospective, what makes u indetermined is the displacement associated to the rigid body motion. One possible solution is to separate rigid (u_R) and elastic displacement (u_E) contributions and to study them separately.

To separate the rigid displacement contribution, associated to the inertia force, its necessary to perform a projection over a modal basis. By projecting the structural displacement on to the rigid modes $\mathbf{\Phi_R}$ and the elastic modes $\mathbf{\Phi_E}$ it is possible to separate the rigid from the elastic contribution.

$$u = u_R + u_E = \mathbf{\Phi_R} q_R + \mathbf{\Phi_E} q_E \tag{3}$$

by left multiplying everything by the transpose of the rigid modes times the mass matrix ($\mathbf{M}$), it is possible to use the orthogonality of the modes with respect to the mass matrix and determine the generalized coordinate associated to the rigid modes.

$$\mathbf{\Phi_R^T} M u = \mathbf{\Phi_R^T} M \mathbf{\Phi_R} q_R + \underbrace{\mathbf{\Phi_R^T} M \mathbf{\Phi_E}}_{0} q_E \tag{4}$$

$$q_R = (\mathbf{\Phi_R^T} M \mathbf{\Phi_R})^{-1} \mathbf{\Phi_R^T} M u \tag{5}$$

It is now possible to identify the elastic component associated to the displacement as:

$$u_E = u - u_R = u - \mathbf{\Phi_R} q_R \tag{6}$$

The rigid degrees of freedom associated to the free-free aircraft are three translations and three rotations. By considering only symmetric steady flight conditions, out of those six degrees of freedom only the rotations due to a change in the angle of attack of the aircraft (α) has an influence over aerodynamic performances. Therefore we could rewrite Eq. 1 as:

$$\widehat{C}_D \approx f\left(\alpha\left(X\right), u_E\left(X\right)\right) \tag{7}$$

In order to take into account in the surrogate model of the structure of the elastic displacement, an approximation of the displacement is performed with a projection-based reduced-order model:

$$u_E \approx \tilde{\mathbf{\Phi}}_E q_E \tag{8}$$

where, instead of using the general modal basis $\mathbf{\Phi}_E$ with infinite number of basis vectors Φ_i, the truncated modal basis $\tilde{\mathbf{\Phi}}_E$ with finite number of modes n in used (i.e. $\tilde{\mathbf{\Phi}}_E = [\Phi_1 \ \Phi_2 \ ... \ \Phi_n]$). To obtain the values of the elastic generalized coordinates (q_E) the least squares problem (10) need to be solved.

$$q_E^* = \min_{q_E} \left|\left| u_E - \tilde{\mathbf{\Phi}}_E q_E \right|\right|_K^2 \tag{9}$$

where K is the stiffness matrix and $||.||_K$ correspond to the norm calculated in the space K. Equation 10 can be solved using:

$$\left(\tilde{\mathbf{\Phi}}_E^T K \tilde{\mathbf{\Phi}}_E\right) q_E^* = \tilde{\mathbf{\Phi}}_E^T K u_E \tag{10}$$

It is then possible to rewrite the surrogate model as:

$$\widehat{C}_D \approx f\left(\alpha\left(X\right), \tilde{\mathbf{\Phi}}_E\left(X\right), q_E^*\left(X\right)\right) \tag{11}$$

In order to further simplify the surrogate model and to make it independent from the projection matrix $\tilde{\mathbf{\Phi}}_E$, the projection matrix is considered fixed and kept constant during the optimization. By doing so we make the assumption that any structural displacement, at which the structure is subjected to during the optimization, can be projected over a constant projection basis ($\overline{\mathbf{\Phi}}_E$) without leading to significant displacement residual ($u_{RES} = ||u - \overline{\mathbf{\Phi}}_E q_E^*||_K^2$). A set of the first 50 structural modes obtained from a previously optimized structure has been selected to build the constant projection basis. The reason behind using so many modes comes from the need to reduce as much as possible the residual error of the displacement. This is important if a the assumption of negligible u_{RES} need to be valid. At this point the surrogate model can be represented as:

$$\widehat{C}_D \approx f\left(\alpha\left(X\right), q_E^*\left(X\right)\right) \tag{12}$$

With Eq. 12 all information needed by the surrogate model about the wing displacement are condensed into the angle of attack, a constant projection basis and 50 generalized coordinates. Nevertheless, building a surrogate with 51 variable that could be correlated it is not ideal. Therefore, we decided to perform a principle component analysis (PCA) to convert a set of possibly correlated variables in to a new set of uncorrelated variables (v) on a new orthogonal coordinate system. Using uncorrelated variables results in better surrogate model training and reduces possible numerical issues.

The PCA is an orthogonal linear transformation that transform a the data to a new coordinate system such that the first vector basis, or principal modes of variation, is aligned with along the direction where data have the largest variance (Figure 1). The second vector basis, and all the succeeding

one, points to the highest variance possible under the constraint the new vector is orthogonal to the preceding components. The resulting vectors form an orthogonal basis set.
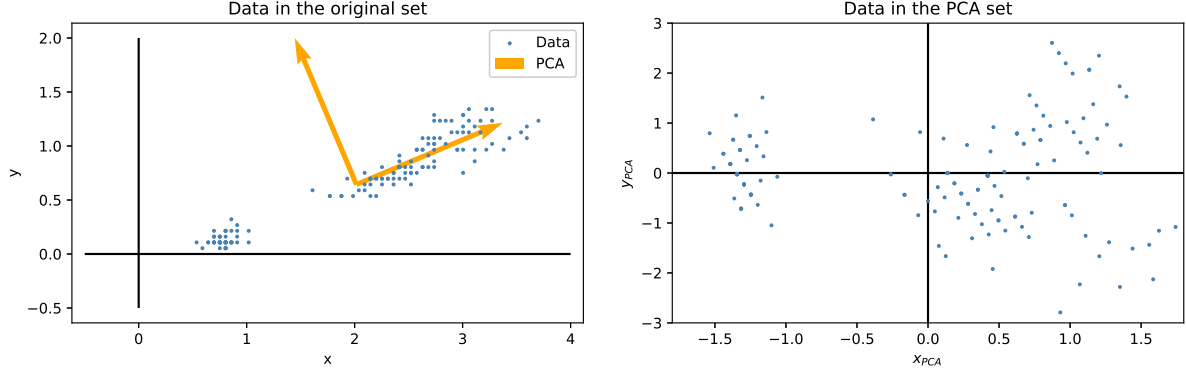

Figure 1: Data in the the original coordinate system with the directions of highest variance of data and the data in PCA coordinate system.

In order to have data on the generalized coordinates associated to the projection of realistic aeroelastic displacements on the constant projection basis $\overline{\mathbf{\Phi}}_E$, an aeroelastic optimization of the same structure is performed and its optimization history has been saved. The performed optimization involved only structural constraints, no aerodynamic performance was involved. The optimization history has been used to extract realistic structural configurations encountered during the optimization. These configurations have been then perturbed with random white noise in order to include a wider range of structures. Once the pool of structures has been generated and perturbed, each of the 150 sampled structures has undergone an aeroelastic analysis that determined the wing displacement at trimmed condition and the generalized coordinates when projected over $\overline{\mathbf{\Phi}}_E$. This process allowed also to define the range of realistic generalized coordinates and angles of attack.

The data obtained with this process have been used to perform a PCA of the generalized coordinates and obtain a reduced set of new PCA coordinates (v) by truncating the principal modes of variation that have the lowest variance. In Figure 2 are reported the correlation matrices of the first 10 generalized coordinates (q_E) and the corresponding PCA coordinates (v). The figures clearly show that the generalized coordinates where indeed correlated while the new of coordinates are not. The effect of the PCA selecting basis vectors from the direction of highest variance to the lowest is clearly shown in Figure 3.
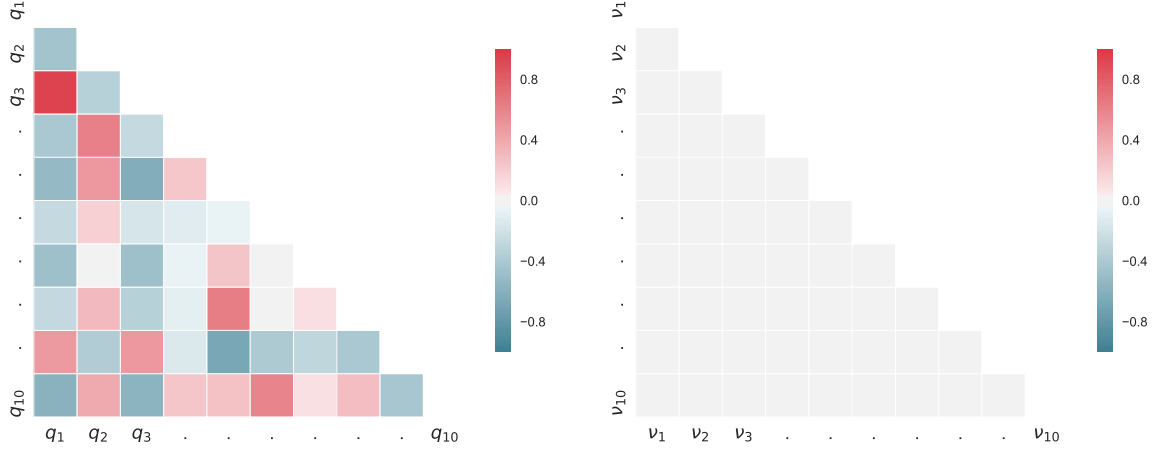
Figure 2: Correlation matrices of the first ten generalized coordinates q_i (on the left) and of the new PCA coordinates ν_i (on the right).
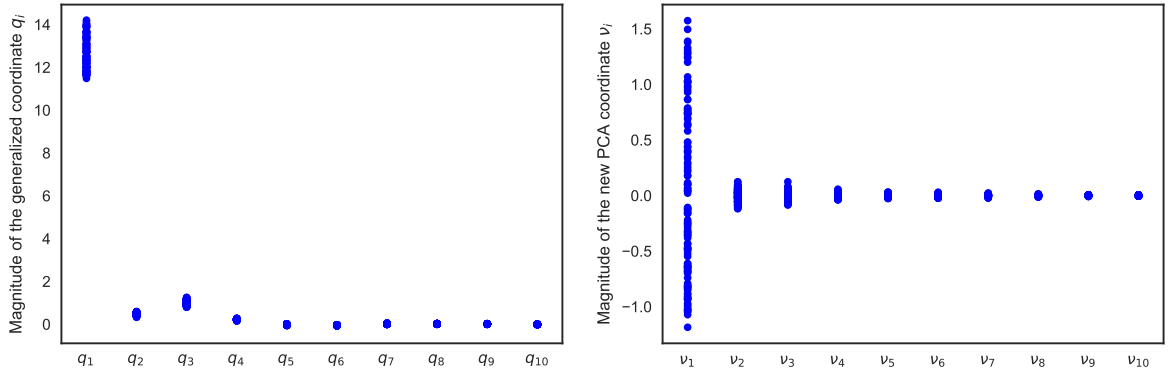

Figure 3: Magnitude of the generalized coordinates q_i and the new PCA coordinates ν_i respectivelly.

Moreover, it has been found (see Figure 4) that just the first two principal modes of variation were sufficient to account for > 99.6% of the data variance ($\sum_{i=1}^{n} \sigma_i^2/\sigma_1^2$, where σ_i is the variance associated to the ith PCA direction). This significantly reduces the amount of input to the surrogate model and also its complexity. The first two principal modes of variation are presented in a magnified way in Figure 5. Therefore, the original Eq. 1 can be rewritten as:

$$\widehat{C}_D \approx f\left(\alpha\left(X\right), \nu_1\left(X\right), \nu_2\left(X\right)\right) \tag{13}$$

In Eq. 13 the effect the structural parameters, like panel thickness and composite anisotropy, over the aerodynamic performance is translated in the effect of these three parameters. These parameters, or surrogate variables, are the angle of attack (α), that takes into account for wing rigid body motion, and two parameters (ν_1 and ν_2) derived from the structural generalized coordinate via PCA.
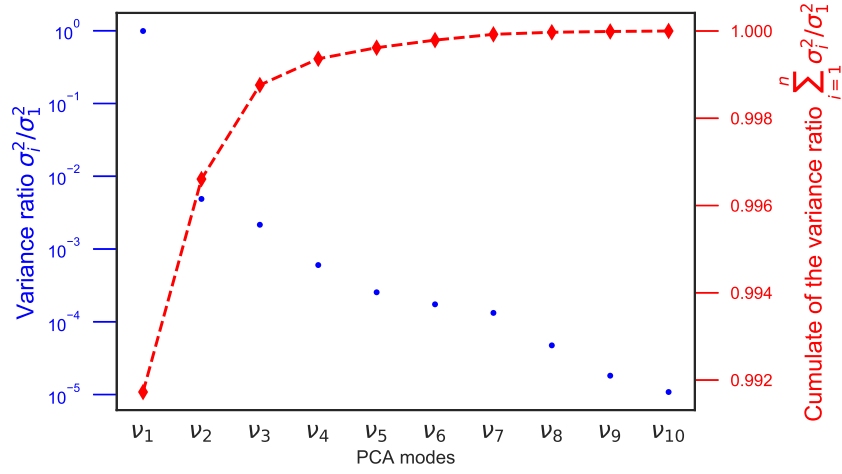
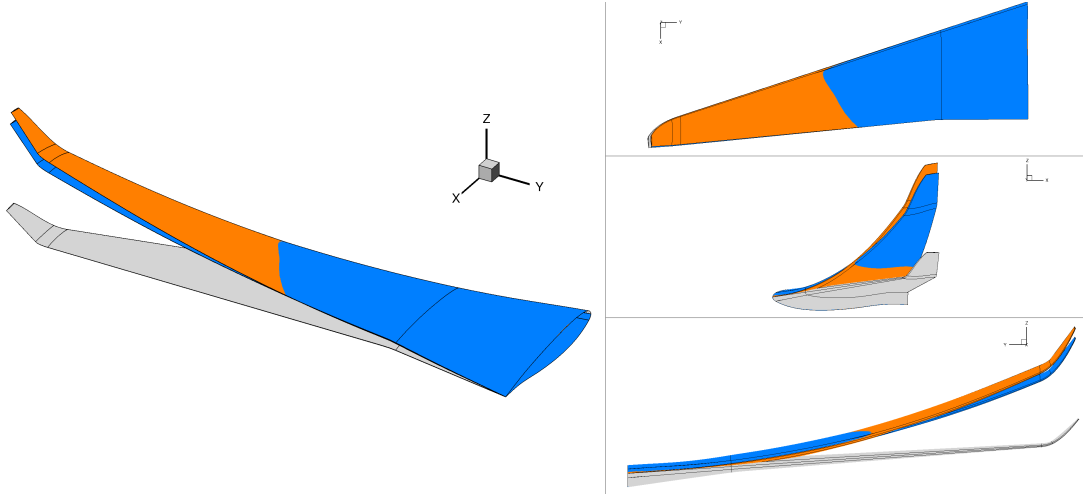Figure 4: Variance ratio for each of the first 10 PCA modes and the cumulate value.

Figure 5: Visualization of the PCA modes. Original wing in gray, magnified mode associated to PCA component ν_1 in orange and magnified mode associated to PCA component ν_2 in blue.

2.2   Surrogate Model

In this section the DOE strategy adopted for the creation of the surrogate model is presented together with a brief introduction of the models considered in the building of the surrogate. The selection criteria and the surrogates performance are shown and finally the best performing surrogate is chosen.

2.2.1   Design of Experiments

As mentioned in Sec. 2.1, a set of feasible structures has been retrieved from a former structural optimization and the corresponding aeroelastic displacements have been transformed into generalized coordinates and, via principal component analysis, into new PCA variables (ν). By doing so a realistic range of the three surrogate variables (α, ν_1 and ν_2) is obtained. The obtained range have been then doubled in order to take into account for a wider range of displacements. To evenly sample the new

design space (Figure 6), the Halton sequence is used. This sequence is deterministic but thanks to its low discrepancy property it can sample uniformly the design space.
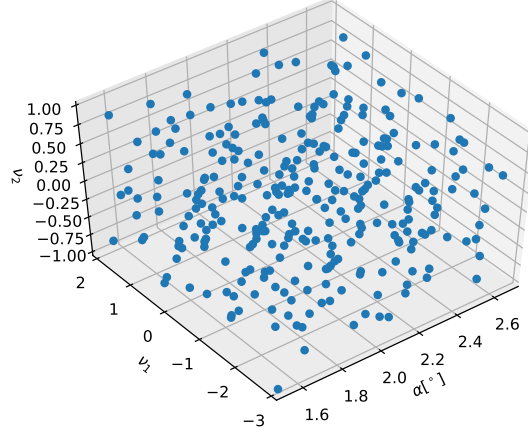

Figure 6: Sample scheme in the PCA space (v_1 vs v_2).

After the DOE the sampled v_1 and v_2 are converted into generalized coordinates $q = [q_1, q_2, ..., q_{50}]$ and then into elastic displacement $u_E \approx \tilde{\Phi}_E q_E$. This structural displacement is splined, by means of Thin Plate Spline (TPS), onto the aerodynamic wetted surface and then the aerodynamic mesh is deformed accordingly using *elsA*. The corresponding α then used in the CFD computation and the resulting lift and drag coefficients for each configuration sample are stored for surrogate model constructions.

Figure 7 shows the correlation between surrogate inputs (α, v_1 and v_2) and outputs (C_L and C_D). As usually desired, inputs are not correlated. Moreover, it is clear that the α has greater influence over C_L and C_D then the two PCA coordinates. The range of the outputs is portrayed in Figure 8.
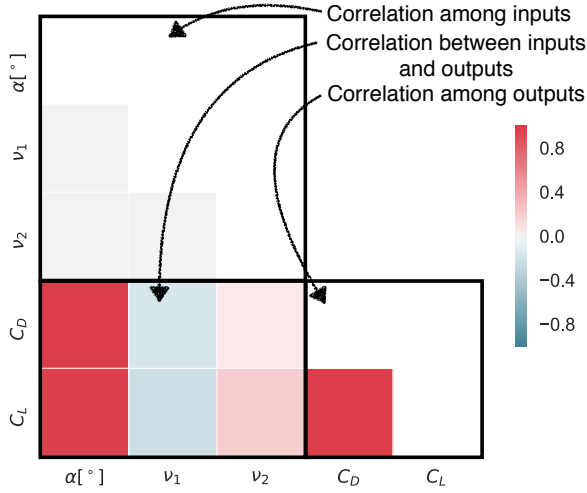
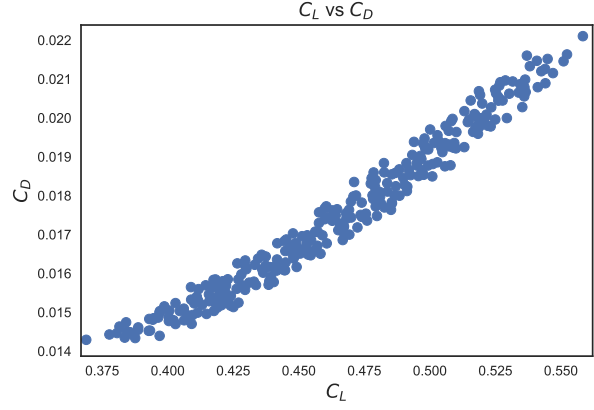Figure 7: Correlation matrix between inputs and outputs of the surrogate model.

Figure 8: Sampled C_D vs C_L space.

2.2.2 Models considered

For this exploratory work only few simple surrogate models are investigated: linear regression (LR), polynomial regression (PR) and Support Vector Machine (SVM) with RBF kernel. The selection of the most suitable model is carried out by comparing: cross validation error and the regression error characteristics (REC) [2] area. Another factor that should be taken into account, in case of more sophisticated models, is the ease of implementation inside commercial optimizers (i.e. MSC.Nastran) as LR and PR provides a simple closed form equation, while SVM can results in significant longer formulas.

Linear regression of dimension n creates a linear model that can be represented as:

$$\hat{y} = w_0 + w_1 x_1 + w_2 x_2 + ... + w_n x_n \qquad (14)$$

no hyper-parameters are involved in the model.

Polynomial regression is used when non-linear behavior between input and output, or interaction between inputs, need to be modeled. For the case of dimension 1 and polynomial order k, the regression can be written as:

$$\hat{y} = w_0 + w_1 x_1 + w_2 x_1^2 + w_3 x_1^3 + ... + w_k x_1^k + w_{k+1} x_1 x_2 + ... \qquad (15)$$

where the order k is an hyper-parameters and need to be set before the training of the model.

Support vector regression is a supervised learning model derived from support vector machine method for classification by Vapnik [18]. SVR exists in a linear formulation, a non-linear formulation with kernel functions. In the current work SVR is used together with the RBF kernel. In total three hyper-paramenters need to be set: ϵ (specify the tube within which no penalty is associated), γ (coefficient in the RBF kernel) and C (a penalty parameter that is used for regularization).

2.2.3 Surrogate performance

The selection of the hyper-parametes of the polynomial regression and the SVR is performed through the classical cross validation process over a grid search. The resulting hyper-parameters are shown in Table 1.

		C_D	C_L/C_D
Surrogate Model	**Hyper-parameter**	**Value**	**Value**
Linear Regression	-	-	-
Polynomial Regression	k	4	4
SVR RBF	γ	1.0E-2	1.0E-2
	ϵ	1.0E-4	1.0E-3
	C	1.0E+3	1.0E+4

Table 1: Best performing hyper-paramenters for the polynomial regression and for SVR with RBF kernel.

Figures 9 and 10 show the REC curves of the three models. The REC curve presents the percentage of the amount of predicted quantities that are below a give relative error (on the x-axis). The ideal surrogate model should have 100% of the predicted outcome at 0% relative error, this mean having a REC composed only by an horizontal line at the 100%. As it is possible to conclude from those figures, for both surrogate models the PR and the SVR are well performing while the LR is not. Table 2 present the cross validation error and the REC area. In conclusion among the three candidates the performance of PR and SVR are quite close and PR of order 4 is chosen due to its simplicity.
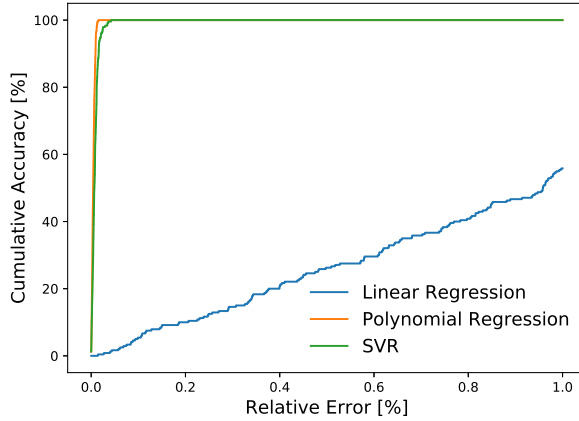

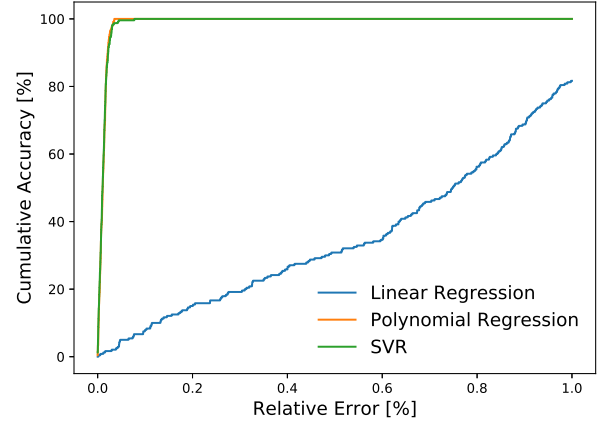Figure 9: Regression Error Characteristics (REC) for C_D surrogate model.

Figure 10: Regression Error Characteristics (REC) for C_L/C_D surrogate model.

	C_D		C_L/C_D	
Surrogate Model	**Cross validation RMSE**	**REC Area**	**Cross validation RMSE**	**REC Area**
Linear Regression	30.323%	25.74	25.887620%	34.62
Polynomial Regression	0.000094%	99.46	0.358646%	98.78
SVR RBF	0.000183%	99.11	0.385440%	98.76

Table 2: Cross validation error and REC area for the different surrogate models.

3 Test case

An ONERA internal wing model is used as a test case for this paper. The FEM model and the aerodynamic CFD skin are presented in Figure 11.
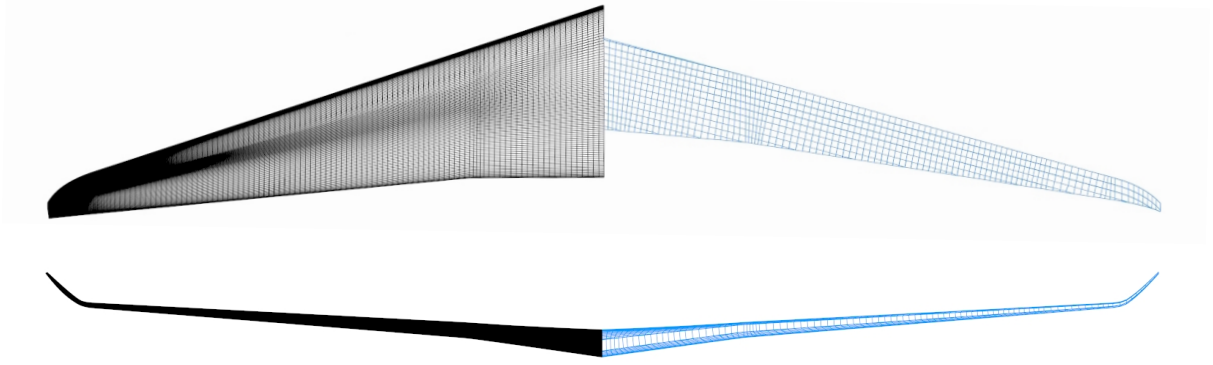

Figure 11: Top and back view of the wing skin aerodynamic mesh (in black) and the structural FEM model (in blue).

3.1 Structural Model Description

The shell FE shell model is characterized by upper and lower skins, front and rear spars, 32 ribs, 13 stringers and represents a realistic aircraft regional aircraft wing. The structure is divided in sections each of them locally optimized by means its thickness and composite material anisotropy. In total there are 44 sections, 14 for each skin and 8 for each spar (Figure 13). Ribs and stiffeners do not take part in the optimization and are made of quasi-isotropic composite. Wing dimensions are presented in Table 3 while fuel distribution is shown in Figure 12.

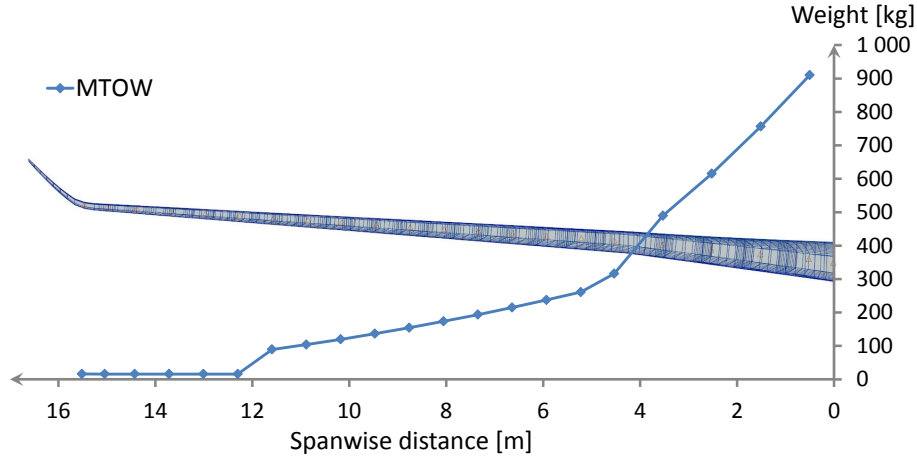| Wing geometric characteristics	
Half Wingspan	16.7 m
Wing Area	111 m^2
Wing Dihedral	3.5°
Leading edge Sweep Angle	18°
MTOW	60,000 kg
Design cruise Mach	0.75

Table 3: Wing features.

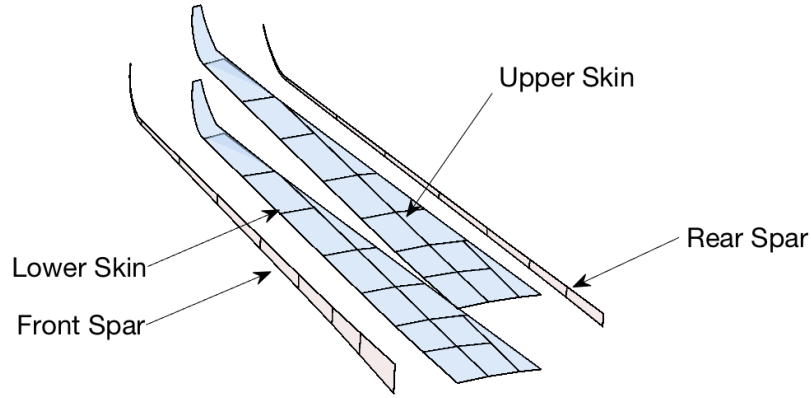Figure 12: Fuel wight distribution over the wing in MTOW configuration.

Figure 13: Wing used in the optimization divided in different sections for local optimization.

3.1.1 Composite parameterization

The composite material used in the model has been parameterized by mean of lamination parameters (LPs). LPs have been first introduced by Tsai et al. [17] and are used to describe the stiffness matrix of composite laminates in a continuous space. Lamination parameters are defined as the integral, over the thickness, of the layers angles (Eq. (16)).In this paper only symmetric stacking sequence are considered, therefore only lamination parameters for membrane (A) and bending (D) stiffness matrices are taken into account.

$$
\begin{aligned}
(V_{1A}, V_{2A}, V_{3A}, V_{4A}) &= \frac{1}{h} \int_{-h/2}^{h/2} (\cos 2\theta, \sin 2\theta, \cos 4\theta, \sin 4\theta) \mathrm{d}z \\
(V_{1D}, V_{2D}, V_{3D}, V_{4D}) &= \frac{12}{h^3} \int_{-h/2}^{h/2} z^2 (\cos 2\theta, \sin 2\theta, \cos 4\theta, \sin 4\theta) \mathrm{d}z
\end{aligned}
\tag{16}
$$

LPs have the advantages of describing the stiffness matrix in a continuos and linear manner (Eqs. (17)) and they define a convex space [8]. Moreover, any generic stacking sequence can be reproduced with twelve continuous variable plus laminate thickness given that each ply is made with

the same material.

$$A = h(\Gamma_0 + \Gamma_1 V_{1A} + \Gamma_2 V_{2A} + \Gamma_3 V_{3A} + \Gamma_4 V_{4A})$$
$$D = \frac{h^3}{12}(\Gamma_0 + \Gamma_1 V_{1D} + \Gamma_2 V_{2D} + \Gamma_3 V_{3D} + \Gamma_4 V_{4D})$$

(17)

where the invariant matrices (Γ_i) contains the UD ply stiffness information by means of the material invariant U_i.

$$\Gamma_0 = \begin{bmatrix} U_1 & U_4 & 0 \\ U_4 & U_1 & 0 \\ 0 & 0 & U_5 \end{bmatrix}, \Gamma_1 = \begin{bmatrix} U_2 & 0 & 0 \\ 0 & -U_2 & 0 \\ 0 & 0 & 0 \end{bmatrix}, \Gamma_2 = \begin{bmatrix} 0 & 0 & U_2/2 \\ 0 & 0 & U_2/2 \\ U_2/2 & U_2/2 & 0 \end{bmatrix},$$

$$\Gamma_3 = \begin{bmatrix} U_3 & -U_3 & 0 \\ -U_3 & U_3 & 0 \\ 0 & 0 & -U_3 \end{bmatrix}, \Gamma_4 = \begin{bmatrix} 0 & 0 & U_3 \\ 0 & 0 & -U_3 \\ U_3 & -U_3 & 0 \end{bmatrix}$$

(18)

On the other hand the use of LPs requires an additional optimization step (usually performed by evolutionary algorithms) that retrieves a discrete stacking sequence from the continuous optimum. The present paper will not consider the stacking sequence retrieval [3] and will focus only on the continuous optimization.

3.1.2 Constraints

Two sets of structural constraints are active on the model. One set of constraints is represented by the material compatibility equations [14], these constraints ensure that each set of in-plane and out-of-plane lamination parameters leads to a realistic "coupled" A and D stiffness matrix. The second set of constraints ensure that the model satisfies mechanical requirements such as strength and local buckling

The strength constraint used have been derived by IJsselmuiden et al. [9] and represent an analytical expressions for a conservative failure envelope based on the Tsai-Wu failure criterion in strain space. Local buckling is constrained via the closed formula Eq. (19) in all regions delimited by two ribs and two stiffeners and is enforced only in the wing skins.

$$\lambda_B = \pi^2 \frac{D_{11}(m/a)^4 + 2(D_{12} + 2D_{33})(m/a)^2(n/b)^2 + D_{22}(n/b)^4}{(m/a)^2 N_X + (n/b)^2 N_Y}$$

(19)

where buckling occurs for $\lambda_B < 1$, N_X and N_Y are the stresses in the longitudinal and transverse directions, a and b are the corresponding region dimensions and m and n are the corresponding number of half waves. The formula do not consider the effects of shear fluxes (i.e. N_{XY}) and non-orthotropic composite bending effects (i.e. D_{13} and D_{23}) into account. A safety margin of 50% is applied to both strength and local buckling criteria.

3.2 Aerodynamic Models

3.2.1 Doublet Lattice Method (DLM)

In this work the aeroelastic loads are calculated via the MSC.Nastran static aeroelastic solver that utilizes doublet lattice method (DLM). Since the aeroelastic loads coming from the DLM are used to

perform trim analysis and to calculate wing displacement, it is important to correctly represent the wing spanwise and chordwise load distribution. This is achieved by using the concept of separation between the rigid and elastic load components, where the DLM rigid part is replaced with rigid CFD results while the elastic increment is computed via DLM. This method, often referred to as Hybrid Static Approach (HSA) [19], allows to consider geometrical effects in the aeroelastic load computation (e.g airfoil camber and wing twist law). This, not only ensures a more realistic lift distribution for structural sizing, but also provide correct wing deflection input to the surrogate model so that the flexible load increment effect on aerodynamic performance will be realistic, thus improving the fidelity of aircraft performance evaluation.

3.3 Computational Fluid Dynamics (CFD)

An aerodynamic mesh with 1M cells is used to perform rigid CFD RANS analysis with Spalart-Allmaras turbulence model. All simulations have been computed at Mach number Ma=0.75 and at an altitude of 35,000 ft. The ONERA CFD solver *elsA* [4] is used to perform all rigid aerodynamic computations.

4 Optimization problem and strategy

Two optimization problems are presented in this work (see (20) and (21)) and formulated as ϵ-constraint problem in order to build the Pareto front point-wise. Both problems aim at reproducing the behavior of conflicting responses like drag coefficient versus wing weight. The objective of the optimization is to control the wing flexibility, which directly effects aerodynamic performance, by increasing wing thickness and tailor composite anisotropy.

$$
\begin{aligned}
\textbf{\textit{Minimize}} \quad & W(X) \\
\textbf{\textit{s.t}} \quad & g(X) < 0 \\
& \widehat{C_D}(X) \leq \overline{C_D}
\end{aligned}
\qquad (20)
$$

$$
\begin{aligned}
\textbf{\textit{Minimize}} \quad & W(X) \\
\textbf{\textit{s.t}} \quad & g(X) < 0 \\
& \widehat{\frac{C_L}{C_D}}(X) \geq \overline{\frac{C_L}{C_D}}
\end{aligned}
\qquad (21)
$$

where X represent the structural parameters and includes thicknesses (t) and composite anisotropy variables ($V_1^A, \dots, V_4^D$) of each section in the structure, $g(x)$ represents mechanical constraints such as strain and buckling and $\overline{C_D}$ and $\overline{\frac{C_L}{C_D}}$ are respectively the target drag coefficient and lift-to-drag ratio. The load cases used in the optimizations are shown in Table 4. It is important to underline that DLM from MSC.Nastran is used in all load cases to generate the aeroelastic loads needed for the optimization. However, while the first two cases (i.e. pull up and push down) are critical for structural sizing they are not very interesting in terms of performance, therefore only the cruise condition is required to fulfill aerodynamic constraints.

N	Name	Mach	Altitude (ft)	Load factor (g)	Surrogate model
1	Pull up	0.48	0	2.5	No
2	Push down	0.48	0	-1	No
3	Cruise	0.75	35000	1	Yes

Table 4: List of load cases used in the optimization.

5   Results and Comments

The results in terms of conflicting responses are presented in Figures 14 and 15. Those figures show two different set of optimizations, in blu the structure has been optimized with respect to both thickness and lamination parameters, while in red a smeared approach has been used freezing the composite anisotropy and using only the thickness as design variable. In both figures it is possible to notice that, tailoring the composite significantly improves wing performance leading to lighter wings. Moreover, when high aerodynamic performance are requires (e.g. small C_D or high C_L/C_D), there is an increment in structural weight and therefore wing rigidity. This, not only underlines the potential benefit of locally tailoring the composite, but also shows the importance of considering aerodynamic performance during aeroelastic structural sizing since not considering them will lead to lighter but undesired designs. The smaller range of improvement in lift-to-drag ratio compared to drag coefficient, is due to the fact that only the wing flexibility, and therefore its structural displacements, is optimized while the aerodynamic shape is kept fixed, limiting the improvements in lift generation.
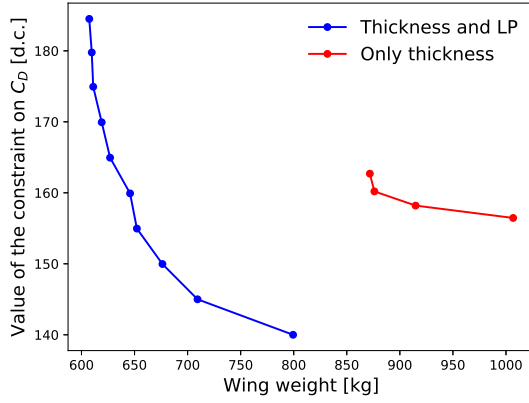

Figure 14: Effect of the constraints on C_D to the optimized weight.
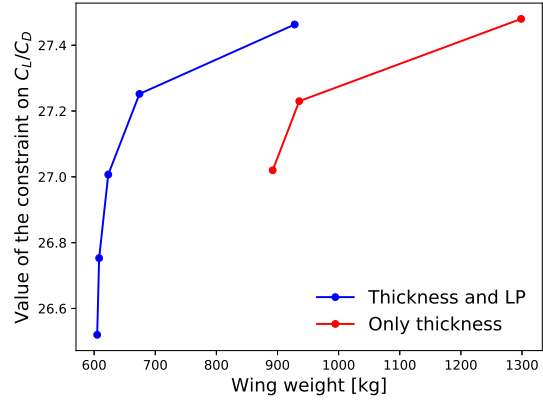
Figure 15: Effect of the constraints on C_L/C_D to the optimized weight.

Effects of the aerodynamic constraints is visible on both composite thickness and anisotropy. Figures 16 and 17 show the thickness distribution of the optimized structures with $C_D = 185$ drag count (d.c.) and $C_D = 140$ d.c. respectively. For the case where the constraint is set to $C_D = 185$ d.c., which is very close to the design without constraint on C_D, most of the thickness is concentrated in the area close to the leading edge and the wing root. This correspond to a structure with higher flexibility in the outboard wing. However, when the constraint is tightened and set to $C_D = 140$ d.c., the overall thickness of the wing is increased and more evenly distributed chordwise. This results in a stiffer wing with respect to both bending and torsion.
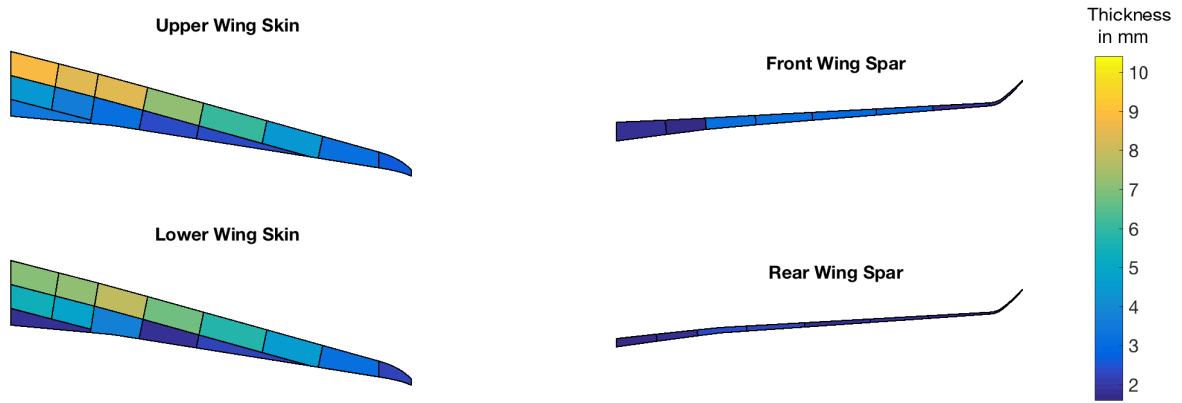
Figure 16: Thickness distribution for the optimized structure with constraint on $C_D = 185$ d.c..
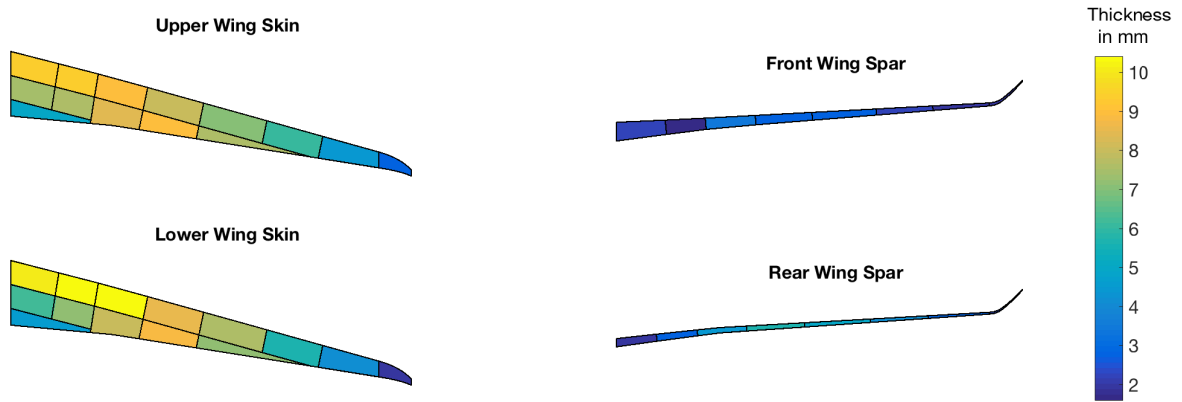

Figure 17: Thickness distribution for the optimized structure with constraint on $C_D = 140$ d.c..

The effect of the aerodynamic constraints over the composite anisotropy distribution is also quite evident. Figures 18 and 19 present the stiffness orientation [5] of the in-plane stiffness component A_{11}. This stiffness distribution allows a visual interpretation of the main fiber direction in each panel. As it is possible to see in Figure 18, where $C_D = 185$ d.c., most of the panels at the wing root and close to the leading edge present a stiffness distribution aligned with the main wing axis direction, this corresponds to a region with high stiffness. The rest of the panels presents a "soft" layout that is keen to create a wash-out effect since most of the fibers in the outer section of the upper wing skin head upwind. In the case where $C_D = 140$ d.c. (Figure 19) most of the panel anisotropy is aligned along the main wing axis, leading to a significantly stiffer structure. In should be pointed out that the outboard section of the upper wing skin has fibers heading downwind while the lower wing skin has fibers heading upwind. At material level this results in a local wash-in effect, as opposed to the wash-out observed when $C_D = 185$ d.c. It is here recalled that neither static divergence not flutter constraints have been considered in this work and that results might change if such constraints would be taken into account.
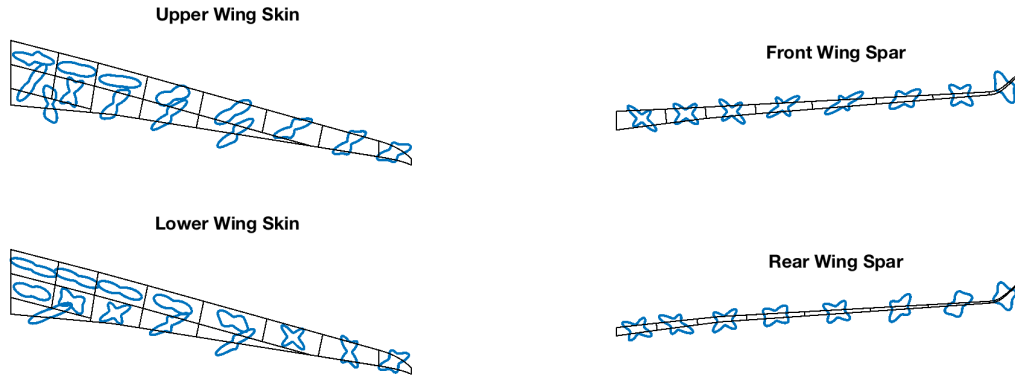
Upper Wing Skin

Front Wing Spar

Lower Wing Skin

Rear Wing Spar

Figure 18: In-plane stiffness distribution along the wing for the optimized structure with constraint on $C_D = 185$ d.c.

Upper Wing Skin

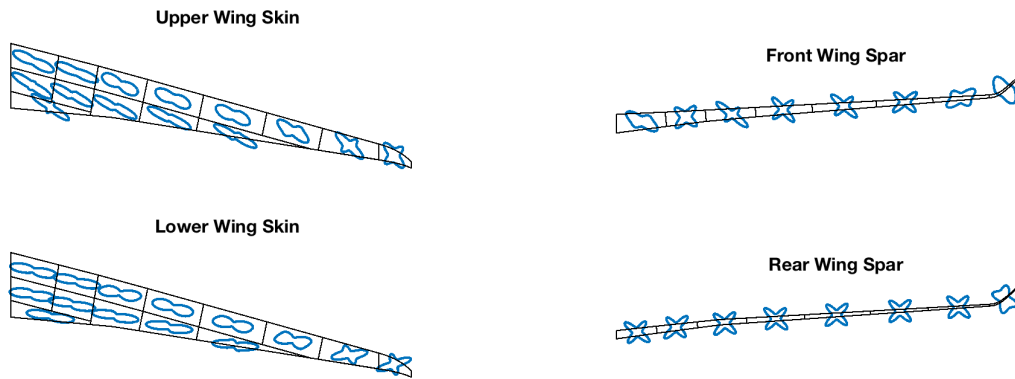**Front Wing Spar**

Lower Wing Skin

Rear Wing Spar

Figure 19: In-plane stiffness distribution along the wing for the optimized structure with constraint on $C_D = 140$ d.c.

The wing behavior expected from the resulting thickness and stiffness distributions is confirmed in figures 20 and 21. The figures show respectively the spanwise change in vertical displacement and the spanwise change in twist between the jig and the flight shape for different structures. The starting point corresponds initial wing configuration prior to optimization, such non-optimized structure has thick panels of non-tailored composite. The results without any constraint over C_D and with $C_D = 185$ d.c. are quite close and show more flexible design in both bending and torsion when compared to the results obtained with $C_D = 140$ d.c.
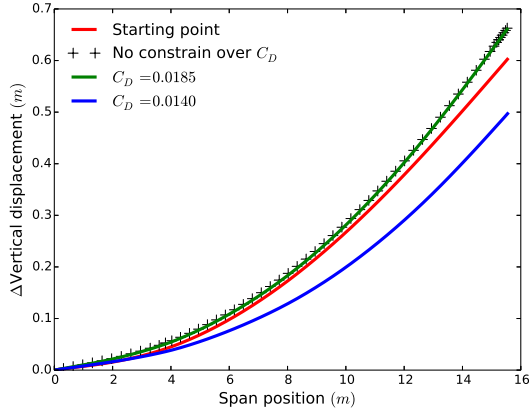
Figure 20: Spanwise change in vertical displacement between jig and flight shape.
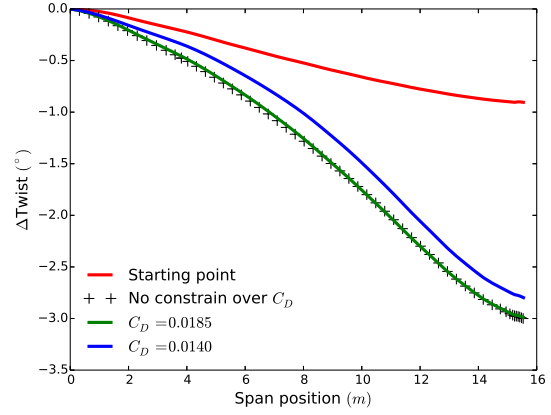

Figure 21: Spanwise change in twist between jig and flight shape.

6   Conclusions and future works

The presented paper proposed an aeroelastic optimization approach capable of performing structural sizing optimization considering both structural and aerodynamic constraints. The approach has been implemented around the FE commercial software MSC.Nastran and utilizes a detailed FE model of a composite wing in order to obtain realistic weight estimation and structural responses. Moreover, a surrogate model based on rigid RANS computations provides a high-fidelity lift and drag coefficient estimation during the optimization. The use of RANS computation allows the surrogate model to represent the total drag and not only the induced drag component.

Convergence history of a previously performed structural optimization, with no aerodynamic performance constraints, is used to approximate the structural displacement on a constant modal projection basis. Moreover, a principal component analysis has been used to reduce the dimension of the input space to only two parameters.

For this exploratory work only few simple surrogate models are investigated: linear regression (LR), polynomial regression (PR) and Support Vector Machine (SVM) with RBF kernel. Results show that a polynomial regression of order four is accurate enough to be used as surrogate model for the drag coefficient and the lift-to-drag ratio. Finally, two optimization problems have been solved under two different aerodynamic constraints (C_D and C_L/C_D). In both cases the approach was able to adequately reproduce the antagonistic nature of the structural and aerodynamic performance indices. Specifically, it is possible to conclude that improvements in aerodynamic performance comes at the price of a heavier and stiffer structure with fixed aerodynamic shape and moreover being able the tailor the composite significantly improves the performance of the structure leading to lighter wings when compared to a smeared composite.

The overall strategy aims at improving distributed MDO architectures. Indeed, such architectures [12] (BLISS, CO, CSSO, ...) often target discipline independency and enhance each discipline optimization problem with interdisciplinary constraints. In this paper, our approach allows the structural optimization problem to be constrained by high fidelity simulation prediction of the aerodynamic

discipline with frozen aerodynamic parameters (i.e. aerodynamic shape). Such a strategy can then be used to reduce discrepancy between each discipline optima and therefore improving the convergence of the overall MDO scheme.

This work on surrogate model will be extended to include winglet planform design. By doing so it would be possible to relieve some of the structural weight penalty for a given aerodynamic constraint by optimizing the winglet planform shape (Figure 22).
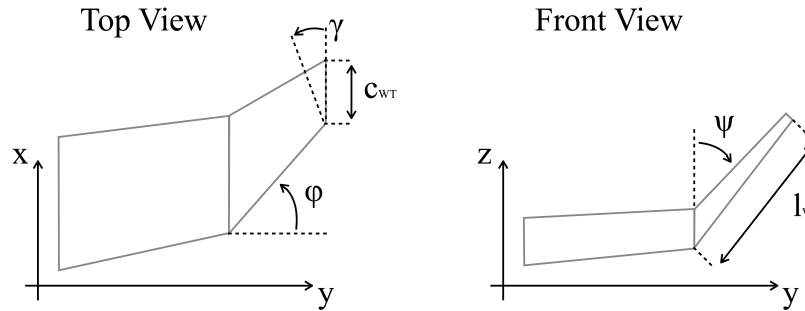

Figure 22: Parameters defining the winglet planform geometry.

References

[1] D. M. Acosta, M. D. Guynn, R. A. Wahls, and R. Del Rosario. Next generation civil transport aircraft design considerations for improving vehicle and system-level efficiency. In *2013 Aviation Technology, Integration, and Operations Conference, AIAA AVIATION Forum, (AIAA 2013-4286)*, 2013.

[2] J. Bi and K.P. Bennett. Regression error characteristic curves. In *Proceedings of the Twentieth Inter?national Conference on Machine Learning ,(ICML-2003)*, pages 43–50, 2003.

[3] M. T. Bordogna, T. Macquart, D. Bettebghor, and R. De Breuker. Aeroelastic optimization of variable stiffness composite wing with blending constraints. In *17th AIAA/ISSMO Multidisciplinary Analysis and Optimization Conference*, June 2016.

[4] L. Cambier, M. Gazaix, S. Heib, S. Plot, M. Poinot, J.-P. Veuillot, J.-F. Boussuge, and M. Montagnac. An overview of the multi-purpose elsa flow solver. *Aerospace Lab Journal*, 2, 2011.

[5] J. K. S. Dillinger. *Static Aeroelastic Optimization of Compisite Wing with Variable Stiffness Laminates.* PhD thesis, Delft University of Technology, 2014.

[6] Charbel Farhat and Michel Géradin. On the general solution by a direct method of a large-scale singular system of linear equations: application to the analysis of floating structures. *International Journal for Numerical Methods in Engineering*, 41(4):675–696, 1998.

[7] J.P. Giesing, T.P. Kalman, and W.P. Rodden. Subsonic unsteady aerodynamics for general configurations. *Tech. Rep. AFFDL-TR-71-5, Part II, Vol. II, Air Force Flight Dynamics Laboratory*, 1972.

[8] J.L. Grenestedt and P. Gudmundson. Layup optimization of composite material structures. In Pauli PEDERSEN, editor, *Optimal Design with Advanced Materials*, pages 311 – 336. Elsevier, Oxford, 1993.

[9] S. T. Ijsselmuiden, M. M. Abdalla, and Z. Gurdal. Implementation of strength-based failure criteria in the lamination parameter design space. *AIAA Journal*, 46(7):1826–1834., 2008.

[10] G. Kenway, G. Kennedy, and J. R. R. A. Martins. Aerostructural optimization of the Common Research Model configuration. In *15th AIAA/ISSMO Multidisciplinary Analysis and Optimization Conference*, June 2014.

[11] Sonia Lebofsky, Eric Ting, Nhan T. Nguyen, and Khanh V. Trinh. *Aeroelastic Modeling and Drag Optimization of Flexible Wing Aircraft with Variable Camber Continuous Trailing Edge Flap*. American Institute of Aeronautics and Astronautics, 2014.

[12] Joaquim R. R. A. Martins and Andrew B. Lambe. Multidisciplinary design optimization: A survey of architectures. *AIAA Journal*, 51(9):2049–2075, 2013.

[13] Ricardo M. Paiva, AndréR. D. Carvalho, Curran Crawford, and Afzal Suleman. Comparison of surrogate models in a multidisciplinary optimization framework for wing design. *AIAA Journal*, 48(5):995–1006, 2010.

[14] G. Raju, Z. Wu, and P. Weaver. On further developments of feasible region of lamination parameters for symmetric composite laminates. In *55th AIAA/ASME/ASCE/AHS/ASC Structures, Structural Dynamics, and Materials Conference, AIAA SciTech, (AIAA 2014-1374)*, 2014.

[15] C.C. Rasmussen, R.A. Canfield, and M. Blair. Optimization process for configuration of flexible joined-wing. *Structural and Multidisciplinary Optimization*, 37(3):265, 2008.

[16] M. H. Shirk, T. J. Hertz, and T. A. Weisshaar. Aeroelastic tailoring - theory, practice, and promise. *Journal of Aircraft*, 23(1):6–18, 1986.

[17] S. W. Tsai and H. T. Hahn. *Introduction to composite materials*. Technomic Publishing Co, 1980.

[18] V Vapnik. *The Nature of Statistical Learning Theory*. Springer, New York, 1995.

[19] Fausto Gill Di Vincenzo. Hybrid static aeroelasticity new capabilities - cfd data management, 06 2012.

[20] Ke-Shi Zhang, Zhong-Hua Han, Wei-Ji Li, and Wen-Ping Song. Coupled aerodynamic/structural optimization of a subsonic transport wing using a surrogate model. *Journal of Aircraft*, 45(6):2167–2171, 2017/05/28 2008.

Acknowledgement